

# Tunable subpicosecond optoelectronic transduction in superlattices of self-assembled ErAs nanoislands

MARTIN GRIEBEL<sup>1</sup>, JURGEN H. SMET<sup>\*1</sup>, DANIEL C. DRISCOLL<sup>2</sup>, JÜRGEN KUHL<sup>1</sup>, CRISTINA ALVAREZ DIEZ<sup>1</sup>, NICOLAS FREYTAG<sup>1</sup>, CHRISTOPH KADOW<sup>2</sup>, ARTHUR C. GOSSARD<sup>2</sup> AND KLAUS VON KLITZING<sup>1</sup>

<sup>1</sup>Max-Planck-Institut für Festkörperforschung, Heisenbergstraße 1, 70569 Stuttgart, Germany

<sup>2</sup>Materials Department, University of California-Santa Barbara, Santa Barbara, California 93106-5050, USA

\*e-mail: j.smet@fkf.mpg.de

Published online 26 January 2003; doi:10.1038/nmat819

In applications as diverse as fibre-optic communications and time-domain or terahertz spectroscopy, researchers are keen on ultrafast optoelectronic transducers that can be tailored to specific needs. The molecular beam epitaxy of photoconductors composed of equidistant layers of self-assembled ErAs-islands in a III-V semiconductor matrix, which act as efficient non-radiative carrier capture sites, enables this flexibility. Here, photocurrent autocorrelation techniques are applied to metal-semiconductor-metal photodetectors patterned on ErAs:GaAs superlattices. The experiments demonstrate that the electrical response speed can be conveniently tuned over at least two orders of magnitude starting from 190 fs by increasing the thickness of the GaAs spacer separating adjacent ErAs layers. The same concept is applied to the narrower bandgap InGaAs matrix. We demonstrate an electron lifetime of approximately 1 ps for this material. This brings closer the prospect of implementing terahertz technology at the important optical communication wavelengths of 1.3 and 1.55  $\mu\text{m}$ .

The inception of semiconductor materials with ultrafast optoelectronic transduction capabilities due to fast carrier trapping has brought within reach a diversity of high-frequency tools and optoelectronic components with unsurpassed bandwidth. Photomixers<sup>1-3</sup> and pulse-driven dipolar antennas<sup>4</sup> fabricated from these materials have been regarded as promising sources of broadly tunable coherent terahertz radiation for use as a local oscillator<sup>5</sup> in submillimetre wave receivers as well as spectroscopy of dielectrics, semiconductors and gases<sup>4,6</sup>. Some of these techniques, such as photomixing, do not only exploit the short carrier lifetime to achieve the highest bandwidths possible, but also rely on the nonlinear behaviour of the photoresponse as a function of the incident optical power. These materials can also be used as photoconductive switches, which serve to detect and inject subpicosecond electrical transients into arbitrary circuits for high-resolution time-domain spectroscopy<sup>7-9</sup>. Advances in terahertz systems gradually open up applications including tomographic and cellular level imaging, biological sensing and label-free genetic analysis<sup>10</sup>. Metal-semiconductor-metal (MSM) photodetectors based on these materials score the highest in terms of response speed<sup>11</sup>, and are considered attractive for front-end receivers in fibre communication, the largest market for fast photodetectors, owing to their low capacitance, straightforward coupling to single mode fibres without compromising bandwidth, and their applicability to monolithic integration with field-effect transistor circuits<sup>12-14</sup>.

Frequently, this diversification in use requires materials whose performance can be tailored to the specific needs of each application. For instance, tunability in the response speed may help MSM photodetectors to reach a better balance with bandwidth limitations of adjacent circuitry while retaining the highest responsivity. More generally, some interdependencies in device parameters are interrupted, so that the design is simplified and devices can be better matched. In this work, we investigated a material composed of equidistant layers of self-assembled ErAs islands incorporated in a high-quality GaAs matrix (ErAs:GaAs) by molecular beam epitaxy<sup>15,16</sup>. We demonstrate that the semimetallic ErAs inclusions act as trapping sites with an intrinsic capture time that is well below 190 fs. By simply changing the distance between the adjacent ErAs layers, the response can be tuned starting from this lower limit over more than two orders of magnitude and

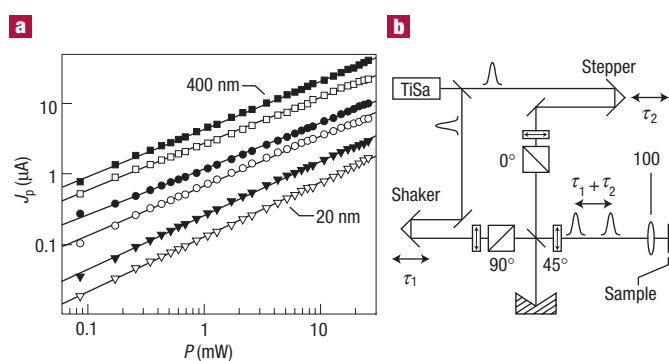


**Figure 1** Nonlinear behaviour of the photocurrent and optical set-up for temporal carrier density autocorrelation measurements. **a**, Photocurrent as a function of the average incident optical power for ErAs:GaAs-based switches with a superlattice period (from bottom to top) of 20, 40, 100, 200, 300 and 400 nm at a bias voltage of 3 V. We roughly estimate the photogenerated carrier density to be  $8 \times 10^{17} \text{ cm}^{-3} \text{ mW}^{-1}$ . **b**, The beam of a mode-locked Ti:Sa laser, tuned to a centre wavelength of 800 nm and producing pulses with a duration of approximately 160 fs at a repetition rate of 76 MHz, is split into two pulse trains. The beams are delayed with respect to each other with the help of a retroreflector, which moves periodically at a frequency of 16 Hz (hereafter referred to as the shaker). After cross-polarizing both pulse trains, they are superimposed collinearly and focused with a 100 $\times$  objective to an approximately 3- $\mu\text{m}$ -diameter spot onto the photoconductive switch. The photocurrent drawn between the biased ends of the CPW is detected with a transimpedance amplifier and recorded with a sampling oscilloscope as a function of the periodically varying time delay. To suppress the intensity noise of the laser system an averaging over some hundred delay cycles is carried out. Delay times not accessible with the shaker are produced with a retroreflector mounted on a stepper motor driven translation stage. Here, the signal-to-noise ratio is improved by mechanically chopping both pulse trains at different frequencies and acquiring the nonlinear part of the photocurrent by sum-frequency lock-in detection.

traded off, if necessary, for improved dark resistance<sup>16</sup>. ErAs:GaAs has excellent surface morphology and is thermally stable up to 700 °C, making it particularly suitable for integration into complex heterostructures<sup>16</sup>, as well as for applications demanding high-power handling capabilities such as photomixing. The dark resistance and trap density are independently accessible through the island size and density, which can be directly controlled by the growth temperature and the amount of ErAs deposited<sup>16</sup>. This contrasts with the sensitivity of the microstructure and response time of low-temperature grown (LTG) GaAs, the most widely used short-lifetime material<sup>17,18</sup>, on any post-growth anneal at temperatures above its own growth temperature.

The idea of inserting layers of self-assembled ErAs dots to engineer optimal dynamical properties can also be extended to smaller bandgap materials such as InGaAs lattice matched to InP<sup>19,20</sup>, which efficiently absorbs at the longer wavelengths of interest to long-haul optical fibre communications. In this work, we demonstrate a response time of approximately 1 ps for a 40-nm period ErAs:InGaAs superlattice, which is largely insensitive to the wavelength of the incident light across the full tunability range of the pulsed laser source used in the experiments. The development of this material is valuable for many laboratory applications too, because it permits experimenters to draw on the large arsenal of commercial fibre-optic components designed for communication wavelengths to construct rugged, compact and user-friendly test and measurement terahertz equipment.

The ErAs:GaAs superlattices are grown by molecular beam epitaxy on (100)-oriented semi-insulating GaAs substrates. After the growth of a 100-nm GaAs buffer layer, the superlattice, consisting of an alternating

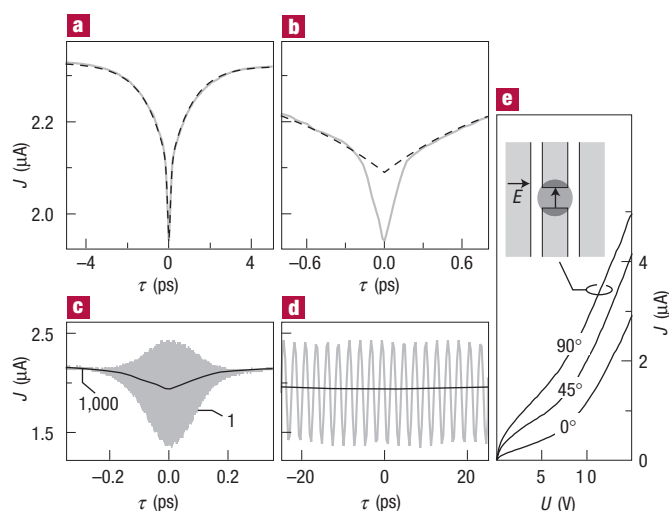


**Figure 2** Photocurrent autocorrelation measurement on a 60-nm ErAs:GaAs superlattice and the polarization-dependent transmission properties of the metal-semiconductor-metal geometry. **a**, Autocorrelation measurement (grey) for a bias voltage of 2.25 V and 0.86 mW of laser light per beam in comparison with a fit (dashed line) to the data using the function described in the text. **b**, The importance of the intensity oscillations caused by the polarization-dependent transmission through the gap is highlighted by comparing the experimental data (grey) with the exponential part of the fit function only (dashed line). **c**, Comparison of the autocorrelation signal obtained when averaging over 1,000 delay cycles (black solid line) and without averaging. To resolve the individual oscillations with the frequency of the laser light, the timescale is expanded in **d**. **e**, Photocurrent as a function of applied bias voltage for different polarization directions of the laser light electric field. This measurement was performed on a 100-nm superlattice with 1.3 mW of incident power per beam. The inset sketches the orientation of the laser beam electrical field relative to the waveguide gap in the 90° configuration.

sequence of GaAs with a thickness (or period)  $L$  and 1.2 monolayers of ErAs, is deposited at a temperature of 530 °C up to a total thickness between 1.2  $\mu\text{m}$  and 1.8  $\mu\text{m}$ . The GaAs layer thickness  $L$  is varied from 10 to 400 nm across a set of nine samples. Under these growth conditions, the nucleation of ErAs on GaAs takes place in a three-dimensional growth mode driven by surface chemistry and produces isolated ErAs islands<sup>15,16</sup> with a size of 1–2 nm and a density of approximately  $7 \times 10^{12} \text{ cm}^{-2}$ . Photoconductive switches are formed by patterning a 3- $\mu\text{m}$  broad gap in the central conductor of a coplanar waveguide (CPW) made out of a 10-nm Ti adhesion layer and a 200-nm Au layer. (A top view and cross section of the samples are shown later in the lower insets of Figs. 3 and 4, respectively.)

Photoconductive switches commonly exhibit nonlinear behaviour in their photocurrent  $J_p$  with incident light intensity or, equivalently, with the density of photoexcited charge carriers  $n$ . Potential sources of this nonlinear behaviour include screening of the external bias field<sup>21–23</sup>, nonlinear capture and recombination terms in the rate equations<sup>24</sup> and/or the electronic circuit topology in which the switch has been embedded<sup>25,26</sup>. Figure 1a illustrates the sublinear power-law dependence of the form  $J_p \propto P^{0.73 \pm 0.08}$ , observed in our ErAs:GaAs-based switches, where  $P$  is the average incident optical power from a single short laser pulse train. The nonlinearity can be exploited to extract the lifetime of the photogenerated mobile charges from autocorrelation experiments<sup>10,21–23,25</sup> in which the time-averaged photocurrent response to the combined light intensity  $I(t, \tau)$  of two cross-polarized optical pulses, one delayed with respect to the other, is recorded as a function of the time delay  $\tau$ , as shown in Fig. 1b. Here,  $t$  is the real time. Both laser

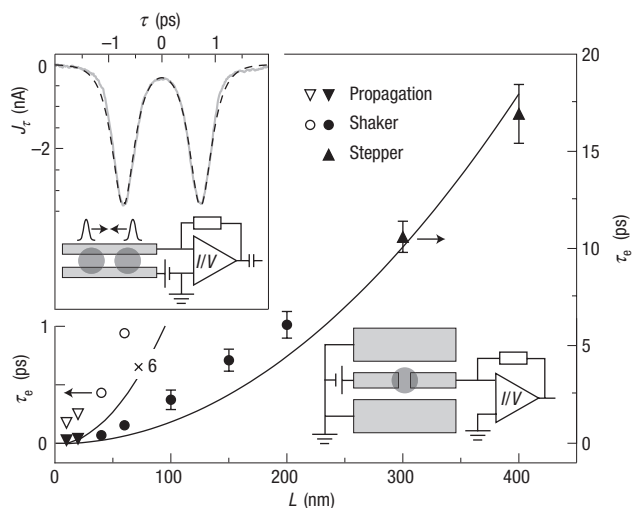


**Figure 3** Lifetime of the photoexcited mobile electrons  $\tau_e$  as a function of the ErAs:GaAs superlattice period  $L$  (right axis, solid symbols). The solid line is a quadratic fit to the data with  $D^* = 9.0 \text{ cm}^2 \text{ s}^{-1}$ . The error bars mark the maximum variation of the electron lifetime observed among a series of 20–60 measurements obtained on different photodiodes from several process runs for the same lattice period. The data points for the smallest periods are replotted as open symbols on the magnified left axis. The upper inset shows a short distance pulse propagation measurement (grey) on a 10-nm ErAs:GaAs superlattice at a bias voltage of 5.0 V and an average power of 1.3 mW per beam.  $J_c$  is the capacitively coupled and delay-dependent contribution to the total current. The 75- $\mu\text{m}$  displacement between the pump and probe beams avoids the cumbersome contribution from the  $\cos\omega t$ -intensity oscillations in autocorrelation experiments. The signal is composed of a double peak structure centred around zero delay that ensues from the coincidence of the right and left incident light beams with electrical pulses that were triggered by the left and right laser pulse trains respectively and have traversed the 75  $\mu\text{m}$  distance. The data can be fit (dashed) with a function derived from an adapted version of equation (1), that takes into account the propagation time and the twofold contribution due to the inverted role of both beams when  $\tau$  changes sign. The lower inset shows the waveguide geometry for photocurrent autocorrelation experiments.

fields are polarized at an angle of  $45^\circ$  with respect to the metallic edges of the CPW to ensure that both beams can be considered equivalent despite diffraction at the waveguide edges<sup>27,28</sup>. The total time-averaged current  $J$ , including both the dark current  $J_d$  and the photocurrent  $J_p$ , is described by<sup>29</sup>

$$J(\tau) = \text{const.} + \frac{1}{T} \frac{d^2 J}{dn^2} \int_{-\infty}^{+\infty} n(t) n(t-\tau) dt, \quad (1)$$

when expanding  $J$  up to second order in  $n(t)$  while ignoring higher-order terms. Here,  $1/T$  is the laser pulse repetition frequency. Because  $d^2 J/dn^2$  is negative, a steep decrease in  $J(\tau)$  is observed near the temporal overlap at  $\tau = 0$  of both laser pulses as seen in Fig. 2a. Owing to their considerably higher mobility in GaAs or InGaAs-based semiconductors, the electrons carry the main part of the current in the photoconductive switches. The hole dynamics plays only a secondary role and its contribution to the photocurrent is neglected in our experiments<sup>22,23</sup>. Because its size is comparable to the laser wavelength, the gap in the CPW acts as a polarization-dependent transmission filter, as confirmed in Fig. 2e. Not unlike wire-grid polarizers in far-infrared and microwave applications, field-components parallel to the metallic edges are therefore attenuated in this geometry. This brings about a rapidly oscillating contribution to  $J(\tau)$ , which is resolved in experiment (Fig. 2c–d) when the customary signal-averaging over many cycles of

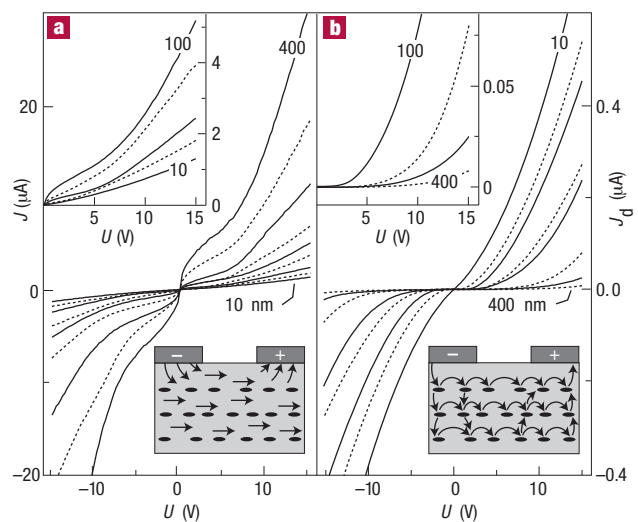


**Figure 4** Current–voltage characteristics of the photoconductive switches when illuminated and in the dark. **a**, Total time-averaged current  $J$  under pulsed-illumination with an average power of 1.3 mW as a function of the applied voltage for ErAs:GaAs-based switches with a superlattice period (from bottom to top) of 10, 20, 40, 60, 100, 150, 200, 300 and 400 nm. The inset in the upper left corner depicts a magnified view for  $L$  between 10 and 100 nm. The lower inset illustrates the free carrier conduction mechanism through the bulk GaAs layers in illuminated switches. **b**, Dark current  $J_d$  as a function of the applied voltage for ErAs:GaAs-based switches with a superlattice period (from bottom to top) of 400, 300, 200, 100, 60, 40, 20 and 10 nm. The inset in the upper left corner shows the dark current on a magnified scale for  $L$  between 400 and 100 nm. The lower inset schematically indicates the hopping conductivity and tunnelling mechanisms responsible for current flow in the non-illuminated switches.

the periodically varying delay  $\tau$  to suppress the influence of laser noise is turned off.

If we take into account these polarization-dependent optical transmission properties of the waveguide gap as well as the signal-averaging and assume electron trapping through a single exponential channel with the lifetime  $\tau_e$ , a suitable functional dependence of  $J$  on  $\tau$  is obtained that permits the extraction of the electron lifetime  $\tau_e$  from a straightforward fitting procedure to the experimental data,

$$J(\tau) = J_0 + J_e \exp\left(-\left|\frac{\tau}{\tau_e}\right|\right) + J_s \operatorname{sech}^2\left(\frac{\tau - \tau_0}{\frac{\lambda}{v_s}}\right). \quad (2)$$

The origin of the various parameters in this equation and the detailed derivation is deferred to the Methods section. An example of the good agreement that can be obtained between the fit function of equation (2) and the experimental data are depicted in Fig. 2a for  $L = 60$  nm. Here, we extract an electron lifetime  $\tau_e = 1.06$  ps. Figure 2b shows exclusively the exponential contribution to emphasize the importance of the last term in equation (2) associated with the polarization-dependent transmission properties of the gap. It may have been overlooked in part of the literature and gives rise to a severe underestimation of  $\tau_e$  if disregarded.

Figure 3 summarizes results for nine different superlattice periods,  $L$ . The electron lifetime can be tuned over two orders of magnitude from 190 fs to 17 ps merely by changing  $L$  from 10 nm to 400 nm, while leaving all other growth parameters fixed. For lattice periods below 40 nm, the hyperbolic secant term of equation (2) overwhelms and masks the exponential term. In this case, we resorted to pulse propagation along a coplanar stripline to evaluate the electron lifetime as illustrated in the inset of Fig. 3. This technique complements the

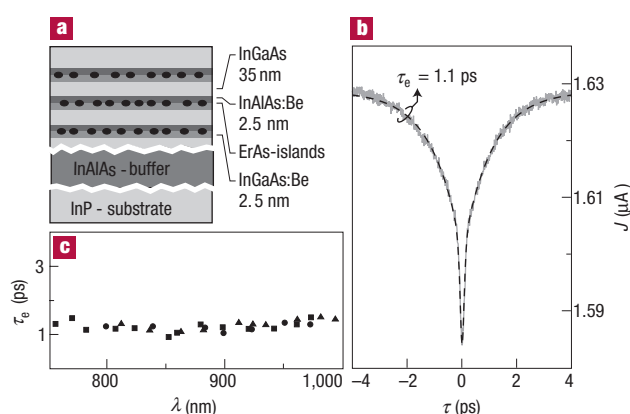


**Figure 5** Device structure of and lifetime measurements on 40 nm period ErAs:InGaAs samples. **a**, After the growth of an  $\text{In}_{0.52}\text{Al}_{0.48}\text{As}$  buffer layer on a semi-insulating InP substrate, an alternating sequence of 35 nm undoped  $\text{In}_{0.53}\text{Ga}_{0.47}\text{As}$ , 2.5 nm Be-doped  $\text{In}_{0.53}\text{Ga}_{0.47}\text{As}$ , 1.75 monolayers of ErAs, and 2.5 nm Be-doped  $\text{In}_{0.52}\text{Al}_{0.48}\text{As}$  is deposited up to a total thickness of about  $1.2 \mu\text{m}$  at a growth temperature of  $490^\circ\text{C}$ . The structure is terminated with a  $37.5 \text{ nm}$   $\text{In}_{0.53}\text{Ga}_{0.47}\text{As}$  cap layer. Before patterning photoconductive switches, the samples underwent a wet chemical treatment that removes approximately  $30 \text{ nm}$  of material. **b**, Autocorrelation measurement (grey line) for a bias voltage of  $2.0 \text{ V}$  and an average power of  $0.86 \text{ mW}$  per beam. The dashed line is a fit to the data with the function described in the text. **c**, Wavelength dependence of the electron lifetime on a number of different switches (denoted by the various symbols) fabricated from the same wafer.

autocorrelation, because it avoids the undesirable signal contributions from polarization-dependent transmission properties through the gap; however, this technique is only applicable for short lifetimes where the propagation distance can be kept small to ensure that waveguide dispersion can be neglected and yet a well-separated double peak signal structure is maintained.

Contrary to LTG-GaAs where the trapping centres are homogeneously distributed and the Shockley–Read–Hall theory<sup>30,31</sup> applies, the localization of defect sites to periodically spaced planes in ErAs:GaAs converts the carrier capture of mobile photoexcited charge carriers into a two-stage process. Diffusion towards a contiguous plane of ErAs islands precedes the impingement on one of the ErAs inclusions and the subsequent immobilization. The diffusive force along the growth direction originates mainly from the large density gradient in the vicinity of these ErAs planes. Note that drift due to the external imposed electric field should proceed mainly in the plane. Under the assumption of a homogeneous in-plane carrier distribution and instantaneous trapping at the ErAs layers with an island separation small in comparison with the superlattice period, the problem reduces to the solution of a one-dimensional ambipolar diffusion equation with the boundary conditions  $n(jL, t) = 0$  for  $t > 0$  (period index  $j = 0, 1, 2, \dots$ ). The incident laser light initially sets up an exponentially decaying distribution of photoexcited charge carriers along the vertical growth direction  $z$  in accordance with Beer's absorption law:  $n(z, t = 0) = n_s \exp(-z/a)$ . Here,  $n_s$  is the initial carrier density at the sample surface and  $a$  is the absorption length of ErAs:GaAs. The leading order terms of a sine expansion yield the following expression for the electron density  $\bar{n}_j(t)$  averaged over super-lattice period  $j$ .

$$\bar{n}_j(t) = \frac{4n_s}{1 + \left(\frac{\pi\alpha}{L}\right)^2} \left(\frac{\alpha}{L}\right)^2 \exp\left(-j\frac{L}{\alpha}\right) \left[1 + \exp\left(-\frac{L}{\alpha}\right)\right] \exp\left(-\frac{\pi^2 D^*}{L^2} t\right). \quad (3)$$

This electron density decays exponentially with a lifetime equal to  $L^2/\pi^2 D^*$ , where  $D^*$  is the ambipolar diffusion constant. A reasonable

value of  $9.0 \pm 0.5 \text{ cm}^2 \text{ s}^{-1}$  for  $D^*$  ensues from the application of this model to the data in Fig. 3. The predicted zero lifetime as  $L$  approaches zero can be traced back to the unphysical assumption of instantaneous carrier trapping at the ErAs planes. It should be noted that a power law fit to the data favours an exponent of 1.5 instead of the quadratic dependence on the superlattice period predicted by this straightforward diffusion model. The key mechanisms responsible for this deviation remain elusive. Saturation of trap sites apparently cannot account for it. If we allow for the possibility that the reduced number of ErAs related trap sites per unit volume for longer superlattice periods is unable to absorb the photoexcited carriers as efficiently due to partial blocking and saturation, we would intuitively anticipate the opposite behaviour. It would result in an even stronger than quadratic rise of the electron lifetime as the superlattice period is increased for the constant excitation density employed in experiment. For the sake of completeness, we note that the electron lifetime does increase as a function of the excitation power: for instance for  $L = 60 \text{ nm}$  with a slope of approximately  $30 \text{ fs mW}^{-1}$  for  $P > 3.5 \text{ mW}$  per beam. Also, experiment reveals that the lifetime rises linearly with applied bias voltage, although much weaker than in our LTG-GaAs reference samples. A more detailed description of the strong non-equilibrium dynamics that explains these dependencies is beyond our scope. It can presumably only be dealt with satisfactorily in a numerical or Monte Carlo approach, which takes into account in a self-consistent manner drift, diffusion, screening, the field- and energy-dependent capture cross section, as well as detailed rate equations.

The dependence of the electron lifetime on the superlattice period is also reflected in the magnitude of the d.c.-photocurrent (Fig. 4a). Current flow proceeds mainly through the bulk GaAs regions and is roughly proportional to the electron lifetime extracted from the autocorrelation experiments. In the dark (Fig. 4b), current flow is mainly confined to the ErAs-island layers and carried by hopping conduction between neighbouring traps. Because the electric field decays rapidly with distance from the semiconductor crystal surface, only the top ErAs island layers contribute, and their number drops with increasing lattice period. Moreover, at the metallic Schottky contacts, the tunnelling probability for injection and collection of charge carriers rapidly diminishes. Both work together to suppress the dark current with increasing lattice period, the opposite behaviour in comparison with the photocurrent. A reduction in the dark current at the expense of a slower response time can be a valuable trade-off in specific applications.

By narrowing the bandgap of the matrix material surrounding the ErAs island layers, photoconductive switches may be operated at longer wavelengths. InGaAs lattice-matched to InP is particularly attractive. It absorbs at wavelengths up to  $1.67 \mu\text{m}$ , so that the all-important optical communication wavelengths are covered. A typical device structure for a superlattice period of  $40 \text{ nm}$  is depicted in Fig. 5a. Thin InAlAs layers ( $2.5 \text{ nm}$ ) cap the ErAs islands to improve the crystallinity and morphology of the ErAs:InGaAs material<sup>19,20</sup>. Furthermore, the metallic ErAs inclusions in InGaAs no longer pin the Fermi level midgap, but rather cause an undesirable n-type background doping of the surrounding narrow gap InGaAs. Consequently, remedies to suppress the dark current to an acceptable level are mandatory. Here, a compensation scheme with p-type dopants incorporated in  $2.5 \text{ nm}$  thick layers above and below the ErAs islands at a concentration level of  $8 \times 10^{19} \text{ cm}^{-3}$  was successfully adopted<sup>19,20</sup>. Figure 5b displays the photocurrent autocorrelation measurement and reveals an electron lifetime of  $1.1 \text{ ps}$  at  $800 \text{ nm}$ . This lifetime is largely insensitive to the operation wavelength as demonstrated in Fig. 5c for the wavelengths of  $750 \text{ nm}$  to  $1 \mu\text{m}$ , that is, across the full tunability range of the Ti:Sapphire pulsed laser source used in the experiments. In view of the absorption edge of  $\text{In}_{0.53}\text{Ga}_{0.47}\text{As}$ , ultrafast operation can be extended up to  $1.55 \mu\text{m}$ . A further reduction of the lattice period may also push the response time of ErAs:InGaAs into the subpicosecond regime.

The molecular beam epitaxy of self-assembled islands of optically active species like InAs or InP embedded in a semiconductor matrix has long proved its merits for basic studies on light emission and lasing among others. Here, the confinement of optically inactive ErAs islands, which act as efficient non-radiative carrier capture sites, to accurately controllable and periodically spaced planes enables the engineering of ultrafast materials with unprecedented flexibility for a plethora of terahertz applications. Apart from offering a very wide response-time tunability, they overcome some of the adverse properties of other photoconductors related to reproducibility and thermal stability. The demonstration of picosecond response times in the case of  $\text{In}_{0.53}\text{Ga}_{0.47}\text{As}$ -matrix material in this work opens up new vistas for implementing receiver and terahertz technology with the help of  $1.55\ \mu\text{m}$  optical components such as compact user-friendly femtosecond pulsed fibre sources.

## METHODS

Under the assumption that trapping of mobile electrons is characterized by a single time constant  $\tau_e$ , the time evolution of their density  $n(t)$  is proportional to the convolution of the intensity profile  $I(t, \tau)$  with the exponential decay  $\exp(-t/\tau_e)\Theta(t)$ , where  $\Theta(t)$  is the Heaviside step function. The incident optical pulses, one delayed for a time  $\tau$  relative to the other, are cross-polarized at an angle of  $45^\circ$  with respect to the metallic edges of the CPW. They produce an electric field incident at the photoconductive-switch of the form

$$\vec{E}(z, t) = \frac{E_0}{\sqrt{2}} \operatorname{sech}\left(\frac{t}{\tau_s}\right) \cos(kz - \omega t) \begin{pmatrix} 1 \\ 1 \end{pmatrix} + \frac{E_0}{\sqrt{2}} \operatorname{sech}\left(\frac{t-\tau}{\tau_s}\right) \cos(k(z-\Delta z) - \omega t) \begin{pmatrix} -1 \\ 1 \end{pmatrix}, \quad (4)$$

where  $E_0$ ,  $\tau_s$ ,  $k$ , and  $\omega$  are the field-amplitude, the characteristic width of the hyperbolic secant-shaped laser pulses, and the wavevector and frequency of the laser radiation, respectively. The second term describes the delayed pulse, which traverses an extra path length of  $\Delta z = c\tau$  (where  $c$  is the vacuum speed of light). This produces an additional phase shift  $k\Delta z$ . Taking into account the attenuation of field components parallel to the metallic edges of the switch, the intensity  $I(t, \tau)$  transmitted through the gap is given by

$$I(t, \tau) = \frac{\epsilon_0 c}{4} E_0^2 \left[ (S_1^2(t) + S_2^2(t)) (\partial^2 + 1) + 2S_1(t)S_2(t)(\partial^2 - 1) \cos \omega\tau \right] \quad (5)$$

where  $\epsilon_0$  is the dielectric constant of vacuum,  $S_1(t) = \operatorname{sech}(t/\tau_s)$ , and  $S_2(t) = S_1(t-\tau)$ . The parameter  $\partial < 1$  captures the damping of the parallel field components, bringing about the rapidly oscillating  $\cos \omega\tau$  term in equation (5), also resolved in experiment (Fig. 2c, d). Note that the careful cross polarisation (Fig. 1b) of the incident laser pulses precludes common interference as its origin. When inserting the convoluted intensity profile of equation (5) for  $n(t)$  in equation (1), the fit function given in equation (2) is obtained. Here,  $J_0$ ,  $J_1$ , and  $J_2$  are the amplitudes of the various signal contributions. Equation (2) has been derived under the assumption that the characteristic width of the laser pulse  $\tau_s$  is much smaller than  $\tau_e$ . The usual averaging over many cycles of the periodic delay time  $\tau$  is accounted for by averaging over one period,  $2\pi/\omega$ , of the laser light. The non-oscillating term in  $I(t, \tau)$  then generates the double-sided single exponential decay term. The time-shifted squared hyperbolic secant, with an effective width  $\hat{\tau}_s$  emanates from the oscillatory part of  $I(t, \tau)$  as an approximation of the resulting double integral by a suitable explicit function.  $\hat{\tau}_s$  is found to be of the order of  $\tau_s \approx 90$  fs in all experiments.

Received 27 September 2002; accepted 29 November 2002; published 26 January 2003.

## References

- Verghese, S. *et al.* Generation and detection of coherent terahertz waves using two photomixers. *Appl. Phys. Lett.* **73**, 3824–3826 (1998).
- McIntosh, K. A. *et al.* Terahertz photomixing with diode lasers in low-temperature-grown GaAs. *Appl. Phys. Lett.* **67**, 3844–3846 (1995).
- Kadow, C., Jackson, A. W., Gossard, A. C., Matsuura, S. & Blake, G. A. Self-assembled ErAs islands in GaAs for optical-heterodyne THz generation. *Appl. Phys. Lett.* **76**, 3510–3512 (2000).
- Grischkowsky, D., Keiding, S., van Exter, M. & Fittinger, C. Far-infrared time-domain spectroscopy with terahertz beams of dielectrics and semiconductors. *J. Opt. Soc. Am. B* **7**, 2006–2015 (1990).
- Verghese, S., McIntosh, K. A. & Brown, E. R. Highly tunable fibre-coupled photomixers with coherent

- terahertz output power. *IEEE Trans. Microwave Theory* **45**, 1301–1309 (1997).
- Chen, P. *et al.* Spectroscopic applications and frequency locking of THz photomixing with distributed-Bragg-reflector diode lasers in low-temperature-grown GaAs. *Appl. Phys. Lett.* **71**, 1601–1603 (1997).
- Auston, D. H. Impulse response of photoconductors in transmission lines. *IEEE J. Quantum Electron.* **19**, 639–648 (1983).
- Paulter, N. G., Sinha, D. N., Gibbs, A. J. & Eisenstadt, W. R. Optoelectronic measurements of picosecond electrical pulse propagation in coplanar waveguide transmission lines. *IEEE Trans. Microwave Theory* **37**, 1612–1619 (1989).
- David, G. *et al.* Absolute potential measurements inside microwave digital IC's using a micromachined photoconductive sampling probe. *IEEE Trans. Microwave Theory* **46**, 2330–2337 (1998).
- Ferguson, B. & Zhang, X.-C. Materials for terahertz science and technology. *Nature Mater.* **1**, 26–33 (2002).
- Kordoš, P., Förster, A., Marso, M. & Rüders, F. 550 GHz bandwidth photodetector on low temperature grown molecular-beam epitaxial GaAs. *Electron. Lett.* **34**, 119–120 (1998).
- Burm, J. *et al.* High-frequency, high-efficiency MSM photodetectors. *IEEE J. Quantum Electron.* **31**, 1504–1509 (1995).
- Fay, P. *et al.* A comparative study of integrated photoreceivers using MSM/HEMT and PIN/HEMT technologies. *IEEE Photon. Technol. Lett.* **10**, 582–584 (1998).
- Das, N. R., Basu, P. K. & Deen, M. J., A new approach to the design optimization of HEMT and HBT for maximum gain-bandwidth of MSM-based integrated photoreceiver and its noise performance at  $1.55\ \mu\text{m}$ . *IEEE Trans. Electron Dev.* **47**, 2101–2109 (2000).
- Kadow, C. *et al.* Self-assembled ErAs islands in GaAs: Growth and subpicosecond carrier dynamics. *Appl. Phys. Lett.* **75**, 3548–3550 (1999).
- Kadow, C., Johnson, J. A., Kolstad, K., Ibbetson, J. P. & Gossard, A. C. Growth and microstructure of self-assembled ErAs islands in GaAs. *J. Vac. Sci. Technol. B* **18**, 2197–2203 (2000).
- Look, D. C. Molecular beam epitaxial GaAs grown at low temperatures. *Thin Solid Films* **231**, 61–73 (1993).
- Gupta, S., Whitaker, J. F. & Mourou, G. A. Ultrafast carrier dynamics in III-V semiconductors grown by molecular-beam epitaxy at very low substrate temperatures. *IEEE J. Quantum Electron.* **28**, 2464–2472 (1992).
- Driscoll, D. C., Hanson, M., Kadow, C. & Gossard, A. C. Electronic structure and conduction in a metal-semiconductor digital composite: ErAs:InGaAs. *Appl. Phys. Lett.* **78**, 1703–1705 (2001).
- Driscoll, D. C., Hanson, M., Kadow, C. & Gossard, A. C. Transition to insulating behavior in the metal-semiconductor digital composite ErAs:InGaAs. *J. Vac. Sci. Technol. B* **19**, 1631–1634 (2001).
- Pašiškevičius, V., Deringas, A. & Krotkus, A. Photocurrent nonlinearities in ultrafast optoelectronic switches. *Appl. Phys. Lett.* **63**, 2237–2239 (1993).
- Jacobsen, R. H., Birkelund, K., Holst, T., Jepsen, P. U. & Keiding, S. R. Interpretation of photocurrent correlation measurements used for ultrafast photoconductive switch characterization. *J. Appl. Phys.* **79**, 2649–2657 (1996).
- Brorson, S. D., Zhang, J. & Keiding, S. R. Ultrafast carrier trapping and slow recombination in ion-bombarded silicon on sapphire measured via THz spectroscopy. *Appl. Phys. Lett.* **64**, 2385–2387 (1994).
- Iverson, A. E. & Smith, D. L. Mathematical modelling of photoconductor transient response. *IEEE Trans. Electron Dev.* **34**, 2098–2107 (1987).
- Grigoras, K., Krotkus, A. & Deringas, A. Picosecond lifetime measurement in semiconductor by optoelectronic autocorrelation. *Electron. Lett.* **27**, 1024–1025 (1991).
- Chen, Y., Williamson, S. & Brock, T. 375-GHz-bandwidth photoconductive detector. *Appl. Phys. Lett.* **59**, 1984–1986 (1991).
- Kuta, J. J., van Driel, H. M., Landheer, D. & Adams, J. A. Polarization and wavelength dependence of metal-semiconductor-metal photodetector response. *Appl. Phys. Lett.* **64**, 140–142 (1994).
- Kuta, J. J., van Driel, H. M., Landheer, D. & Feng, Y. Polarization dependence of the temporal response of metal-semiconductor-metal photodetectors. *Appl. Phys. Lett.* **65**, 3146–3148 (1994).
- Carruthers, T. F. & Weller, J. F. Picosecond optical mixing in fast photodetectors. *Appl. Phys. Lett.* **48**, 460–462 (1986).
- Shockley, W. & Read, W. T. Statistics of the recombinations of holes and electrons. *Phys. Rev.* **87**, 835–842 (1952).
- Hall, R. N. Electron-hole recombination in germanium. *Phys. Rev.* **87**, 387 (1952).

## Acknowledgements

The authors thank R. R. Gerhardt for help with the theoretical description of the experiments. They also acknowledge R. A. Wyss for discussions and M.-H. Stapleton for assistance during the experiments. This research has been supported by the German Science Foundation, the Jet Propulsion Laboratory and QUEST.

Correspondence and requests for materials should be addressed to J.H.S.

## Competing financial interests

The authors declare that they have no competing financial interests.